J. Fluid Mech. (2003), *vol.* 477, *pp.* 363–379.
DOI: 10.1017/S0022112002003361 Printed in the United Kingdom

Improved upper bound on the energy dissipation rate in plane Couette flow: the full solution to Busse's problem and the Constantin–Doering–Hopf problem with one-dimensional background field

By S. C. PLASTING AND R. R. KERSWELL
Department of Mathematics, University of Bristol, Bristol, BS8 1TW, UK

(Received 30 May 2002 and in revised form 18 October 2002)

We present an improved upper bound on the energy dissipation rate in plane Couette flow. This is achieved through the numerical solution of the 'background field' variational problem formulated by Constantin and Doering with a one-dimensional unidirectional background field. The upper bound presented here both exhausts the bounding potential of the one-dimensional background field problem and also solves the provably equivalent problem formulated by Busse. The solution is calculated up to asymptotically large Reynolds number where we can estimate that the energy dissipation rate $\varepsilon \leqslant 0.008553$ as $Re \to \infty$ (in units of V^3/d where V is the velocity difference across the plates separated by a distance d and $Re = Vd/\nu$, with ν kinematic viscosity). This represents a 21% improvement over the previous best value due to Nicodemus *et al.* A comparison is drawn between this numerical solution and the so-called multi-alpha asymptotic solutions discovered by Busse.

1. Introduction

One of the few tools available to the theoretician interested in high-Reynolds-number turbulence is a variational approach which strives to produce rigorous inequality information directly from the governing equations. Although over 40 years old (Malkus 1954, 1956; Howard 1963), the approach has enjoyed a resurgence of interest recently with the discovery of a new alternative technique (Doering & Constantin 1992, 1994; Constantin & Doering 1995; Doering & Constantin 1996; Nicodemus, Grossmann & Holthaus 1997*a*) based upon a mathematical device going back to Hopf (1941). This 'background method', as it has been christened, is now known to produce the complementary variational problem to the classical Euler–Lagrange approach pioneered by Howard (1963, 1972, 1990) and Busse (1968*a*, *b*, 1969*a*, *b*, 1970, 1978) (see Kerswell 1997, 1998, 2001). This has been an important development since new rigorous bounds have emerged which have improved previous bounds (those not including incompressibility as a constraint, Howard 1963; Busse 1968*a*) and put other better bound estimates (incorporating incompressibility) on a firmer footing.

This is particularly true in bounding the energy dissipation rate, ε, in the canonical shear flow problem of plane Couette flow. Over thirty years ago, Busse (1970) set up an Euler–Lagrange problem to maximize the energy dissipation rate possible

for a velocity field which satisfied the dynamical constraints of mean momentum balance and the global power balance together with the kinematic constraints of incompressibility and the boundary conditions. Since this proved analytically intractable, he developed a multiple-boundary-layer approach to estimate the asymptotically large Reynolds number limit. Working within the space of almost periodic functions, Busse considered a variational solution consisting of a countable number of Fourier modes with each mode having its own boundary layer structure. Then, using considerable ingenuity, he secured the estimate $\varepsilon_{Busse} \approx 1/99.7$ as $Re \to \infty$ of the true maximum ε_{bound} for these constraints (measured in inviscid units of V^3/d where V is the velocity difference across the plates separated by a distance d and $Re = Vd/\nu$, with ν kinematic viscosity). Although his problem was one of maximization, Busse argued that this estimate was nevertheless a strict upper bound on the true bound ε_{bound} because the terms he neglected as being higher order would all tend to lower the dissipation estimate. Unfortunately, technical difficulties associated with his analysis (the nestled boundary layers do not separate asymptotically in the required distinguished limit) meant that it was unclear how good an estimate this was and in the absence of accompanying numerical solutions, the way forward was uncertain. This, coupled with the complexity of the analysis, meant interest in the approach waned.

However, twenty years later, in the first application of their new method, Doering & Constantin (1992) derived the first clearly rigorous upper bound $\varepsilon \leqslant 1/11.3$ (as $Re \to \infty$) in the plane Couette problem. This was later improved by Gebhardt *et al.* (1995) down to $\varepsilon \leqslant 1/12.7$ by using a better trial background field, and to $\varepsilon \leqslant 1/15.1$ by Nicodemus, Grossmann & Holthaus (1997*a*, *b*) who found a way of further optimizing the formulation. Then Nicodemus, Grossmann & Holthaus (1998*a*, *b*) developed a sophisticated trial function approach to explore the method for finite Re and managed to lower the asymptotic value even further to $\varepsilon \leqslant 1/92.0$ by extensive numerical calculations. By this point, it had become clear that the best bound that could emerge from the Constantin–Doering–Hopf one-dimensional background problem (optimized by Nicodemus *et al.* 1997*a*) corresponded *exactly* with that available in Busse's original problem (Kerswell 1997, 1998). With this realization, the fact that Nicodemus *et al.*'s result was so close to Busse's provided some reassurance that his multiple-boundary-layer technique was effective.

To properly resolve this issue, however, requires a complete solution of the variational problem to find the asymptotic value of ε_{bound}. The main purpose of this paper is to describe this calculation. The optimal variational solution which emerges is compared with Busse's multiple-boundary-layer estimate in order to indicate how effective an analytic tool his approximation is. This has important implications for other variational problems where Busse's technique still offers the only theoretical way of gaining insight but where complementary numerical computations have not been done.

There are also other interesting issues that need to be addressed. First, neither Busse's multiple-boundary-layer ansatz or the trial function approach adopted by Nicodemus *et al.* (1998*a*, *b*), which artificially restricted the form of the background field profile and fluctuation field, were able to allow the precise form of the optimal flow to emerge. Of particular interest is identifying whether the optimal mean flow profile develops a logarithmic-type layer just outside the viscous sublayer near the boundaries thereby mimicking realized flows. One of the motivations behind constructing such variational problems above and beyond the bounds themselves is learning whether the corresponding optimal solution bears any resemblance to realized

flows. If it does in the case of plane Couette flow, then it is reasonable to speculate that the flow may be trying to maximize the energy dissipation or equivalently the momentum transport across the plates. The fact that asymptotically both Busse's trial solution and the Nicodemus *et al.* solution develop a $\frac{1}{4}$-shear across the interior of the flow is highly suggestive that the true optimal solution does also, but neither can say anything about the potentially delicate structure of the optimal solution at the boundary. This issue has recently become more prominent with the realization that the optimal background field for the maximal energy dissipation rate problem also solves a whole suite of neighbouring variational problems addressing more general functionals of the dissipation and its component parts (see Kerswell 2002).

Secondly, it is unclear which of the features of the upper bound for finite Re that emerged in the work of Nicodemus *et al.* (1998*a*) are true to the optimal bound solution. Most notable amongst these is the surprising global minimum in their bound at $Re \approx 740$ (see figure 8 Nicodemus *et al.* 1998*a*). Busse's asymptotic solution indicates that the optimal solution should contain an ever increasing number of wavenumbers in the fluctuation part of the velocity field as Re increases whereas Nicodemus *et al.* allow only two. The influence of this limitation warrants investigation.

Given these motivations, then, we describe how to solve the full one-dimensional background field variational problem completely up to asymptotically large Reynolds numbers. This calculation finally solves an important variational problem first formulated over 30 years ago by Busse (Busse 1970).

2. Formulation of the variational problem

We wish to consider the system of plane Couette flow in which a fluid layer is sheared by two parallel plane plates a distance d apart with constant relative velocity V. The dimensional governing equations are

$$\frac{\partial \boldsymbol{u}^*}{\partial t^*} + \boldsymbol{u}^* \cdot \nabla^* \boldsymbol{u}^* + \nabla^* p^* = \nu \nabla^{*2} \boldsymbol{u}^*, \tag{2.1a}$$

$$\nabla^* \cdot \boldsymbol{u}^* = 0, \quad \boldsymbol{u}^*\left(x^*, y^*, \pm\tfrac{1}{2}d\right) = \mp\tfrac{1}{2}V\widehat{\boldsymbol{x}}, \tag{2.1b}$$

where the starred variables are dimensional variables, ν is the kinematic viscosity, $\widehat{\boldsymbol{x}}$ denotes the unit vector in the x-direction and the parallel plates are positioned at $z^* = \pm\frac{1}{2}d$. The domain of the fluid is the infinite layer $(x^*, y^*, z^*) \in \mathbb{R}^2 \times [-\frac{1}{2}d, \frac{1}{2}d]$ where x is the streamwise, y the spanwise and z the wall-normal coordinate. All variables are assumed periodic in the horizontal directions.

We non-dimensionalize distances by the plate separation d and time by the viscous diffusion time scale d^2/ν so that the equations become

$$\mathcal{N} := \frac{\partial \boldsymbol{u}}{\partial t} + \boldsymbol{u} \cdot \nabla \boldsymbol{u} + \nabla p - \nabla^2 \boldsymbol{u} = \boldsymbol{0}, \tag{2.2a}$$

$$\nabla \cdot \boldsymbol{u} = 0, \quad \boldsymbol{u}\left(x, y, \pm\tfrac{1}{2}\right) = \mp\tfrac{1}{2}Re\,\widehat{\boldsymbol{x}}, \tag{2.2b}$$

where $Re := Vd/\nu$. Defining bulk averaging and horizontal averaging as

$$\langle(\cdot)\rangle := \int_{-1/2}^{+1/2} \mathrm{d}z\, \overline{(\cdot)} := \int_{-1/2}^{+1/2} \mathrm{d}z \lim_{L_x, L_y \to \infty} \frac{1}{4L_x L_y} \int_{-L_x}^{+L_x} \mathrm{d}x \int_{-L_y}^{+L_y} \mathrm{d}y\,(\cdot), \tag{2.3}$$

the non-dimensionalized, long-time-averaged energy dissipation rate per unit mass

may be written as

$$\mathscr{E} := \frac{d^4}{\nu^3} \lim_{T\to\infty} \frac{1}{T} \int_0^T \nu \langle |\nabla^* \boldsymbol{u}^*|^2 \rangle \, \mathrm{d}t = \lim_{T\to\infty} \frac{1}{T} \int_0^T \langle |\nabla \boldsymbol{u}|^2 \rangle \, \mathrm{d}t. \tag{2.4}$$

In terms of inviscid units, where we non-dimensionalize distance by d and time by d/V, this quantity is just

$$\varepsilon := \frac{d}{V^3} \lim_{T\to\infty} \frac{1}{T} \int_0^T \nu \langle |\nabla^* \boldsymbol{u}^*|^2 \rangle \, \mathrm{d}t = \frac{\mathscr{E}}{Re^3}. \tag{2.5}$$

We derive the Constantin–Doering–Hopf variational problem (henceforth abbreviated to CDH) by considering the Lagrangian functional

$$\mathscr{L} := \lim_{T\to\infty} \frac{1}{T} \int_0^T \mathrm{d}t \left\{ \langle |\nabla \boldsymbol{u}|^2 \rangle - \left\langle a\boldsymbol{v} \cdot \left[\frac{\partial \boldsymbol{u}}{\partial t} + \boldsymbol{u}\cdot\nabla\boldsymbol{u} + \nabla p - \nabla^2 \boldsymbol{u} \right] \right\rangle \right\}, \tag{2.6}$$

where the field $a\boldsymbol{v}$ is a Lagrange multiplier which imposes the governing equations and the real constant a is included for comparison with earlier work on the background field method. The objective is to find the maximum stationary value of $\mathscr{L}$ over $\boldsymbol{u}$, $\boldsymbol{v}$ and a which corresponds to the maximum dissipation rate over all possible solutions to the governing equations. In the CDH problem the Lagrange multiplier field $\boldsymbol{v}$ and the velocity field $\boldsymbol{u}$ are connected via a background field ϕ

$$\phi(z)\widehat{\boldsymbol{x}} := \boldsymbol{u}(\boldsymbol{x}, t) - \boldsymbol{v}(\boldsymbol{x}, t), \tag{2.7}$$

where ϕ is a one-dimensional function independent of time which takes the boundary conditions, $\phi(\pm\frac{1}{2}) = \mp\frac{1}{2}Re$. It should be stressed that ϕ is not necessarily equal to the horizontal average of $\boldsymbol{u}$. This decomposition of $\boldsymbol{u}$ into a 'background field' satisfying the boundary conditions and a 'fluctuation field' that is incompressible and satisfies homogeneous boundary conditions is known as the Hopf decomposition (Hopf 1941). By forcing this relationship between $\boldsymbol{u}$ and $\boldsymbol{v}$, the constraints imposed by $\boldsymbol{v}$ are now only the total power balance and horizontally averaged momentum balance in the $\widehat{\boldsymbol{x}}$-direction. This can be seen by substituting $\boldsymbol{v} = \boldsymbol{u} - \phi\widehat{\boldsymbol{x}}$ into (2.6) and rearranging to obtain

$$\mathscr{L} = \lim_{T\to\infty} \frac{1}{T} \int_0^T \mathrm{d}t \left[\langle |\nabla \boldsymbol{u}|^2 \rangle - a \langle \boldsymbol{u}\cdot\mathscr{N} \rangle + \int_{-1/2}^{1/2} a\phi \, \overline{\mathscr{N}_1} \, \mathrm{d}z \right];$$

$\mathscr{N}$ denotes the Navier–Stokes equations (2.2a) with first component $\mathscr{N}_1$, a is the Lagrange multiplier for the total power balance integral for the Navier–Stokes equations and ϕ is the Lagrange multiplier for the horizontally averaged momentum balance in the $\widehat{\boldsymbol{x}}$-direction.

With the change of variables $\boldsymbol{u} = \phi\widehat{\boldsymbol{x}} + \boldsymbol{v}$, $\mathscr{L}$ can be written as

$$\mathscr{L} = \langle \phi'^2 \rangle - \lim_{T\to\infty} \frac{1}{T} \int_0^T \langle a v_1 v_3 \phi' + (a-1)|\nabla \boldsymbol{v}|^2 - (a-2) v_1 \phi'' \rangle \, \mathrm{d}t \tag{2.8}$$

(where implicitly $\nabla\cdot\boldsymbol{v} = 0$). At this stage the key observation is that if ϕ can be chosen such that $\mathscr{L}$ has a maximum over all $\boldsymbol{v}$, then this value will bound the true dissipation rate ε since any realizable $\boldsymbol{u}$ which satisfies the Navier–Stokes equations can still be reached by some $\boldsymbol{v}$. Minimizing the maximum over allowable ϕ then produces the best such upper bound. It turns out that this is equivalent to finding the largest saddle point value of $\mathscr{L}$ (see Kerswell 1998) which can be accomplished by considering only stationary solenoidal fluctuation fields $\boldsymbol{v}$. With $\lim_{T\to\infty}(1/T)$ dropped from (2.8),

the Euler–Lagrange equations for a, ϕ and $\boldsymbol{v}$ are

$$\frac{\delta \mathscr{L}}{\delta a} := -\langle |\nabla \boldsymbol{v}|^2 + \phi' v_1 v_3 - \phi'' v_1 \rangle = 0, \tag{2.9a}$$

$$\frac{\delta \mathscr{L}}{\delta \phi} := -2\phi'' + a\overline{v_1 v_3}' + (a-2)\overline{v_1}'' = 0, \tag{2.9b}$$

$$\frac{\delta \mathscr{L}}{\delta \boldsymbol{v}} := 2(a-1)\nabla^2 \boldsymbol{v} - a\phi' \begin{bmatrix} v_3 \\ 0 \\ v_1 \end{bmatrix} + \nabla p + (a-2)\phi'' \widehat{\boldsymbol{x}} = \boldsymbol{0}. \tag{2.9c}$$

If we take the mean part of equation (2.9c) and use the incompressibility condition on $\boldsymbol{v}$ we discover that the fluctuation field can be split into a mean part $\overline{v_1}(z)\widehat{\boldsymbol{x}}$ and a mean-less part $\widehat{\boldsymbol{v}}$ ($\overline{\widehat{\boldsymbol{v}}} = \boldsymbol{0}$). Equation (2.9$c$) then splits into two equations, one homogeneous and one inhomogeneous, namely

$$\frac{\delta \mathscr{L}}{\delta \widehat{\boldsymbol{v}}} := 2(a-1)\nabla^2 \widehat{\boldsymbol{v}} - a\phi' \begin{bmatrix} \widehat{v}_3 \\ 0 \\ \widehat{v}_1 \end{bmatrix} + \nabla \widehat{p} = \boldsymbol{0}, \tag{2.10a}$$

$$\frac{\delta \mathscr{L}}{\delta \overline{v_1}} := 2(a-1)\overline{v_1}'' + (a-2)\phi'' = 0. \tag{2.10b}$$

This latter equation can be integrated twice to

$$\overline{v_1} = -\frac{a-2}{2(a-1)}[\phi + Re\, z] \tag{2.11}$$

after applying the boundary conditions for ϕ and $\boldsymbol{v}$, so that the mean flow of the optimal field and the background field are connected as follows:

$$\overline{\boldsymbol{u}} = \left[\frac{a}{2(a-1)}(\phi + Re\, z) - Re\, z\right]\widehat{\boldsymbol{x}}. \tag{2.12}$$

Defining a new parameter $\lambda := a/(a-1)$ and rescaling the pressure field $\widehat{p} \to (a-1)\widehat{p}$ we can transform the remaining equations for the optimal field (2.9a), (2.9b) and (2.10a) to

$$\lambda = 2 - \frac{\langle |\nabla \widehat{\boldsymbol{v}}|^2 \rangle}{Re\langle \widehat{v}_1 \widehat{v}_3 \rangle}, \tag{2.13a}$$

$$\tfrac{1}{2}\lambda(\phi' + Re) = \overline{\widehat{v}_1 \widehat{v}_3} - \langle \widehat{v}_1 \widehat{v}_3 \rangle, \tag{2.13b}$$

$$2\nabla^2 \widehat{\boldsymbol{v}} - \lambda\phi' \begin{bmatrix} \widehat{v}_3 \\ 0 \\ \widehat{v}_1 \end{bmatrix} + \nabla \widehat{p} = \boldsymbol{0}, \tag{2.13c}$$

$$\nabla \cdot \widehat{\boldsymbol{v}} = 0, \tag{2.13d}$$

where (2.13a) has been written for optimal numerical conditioning (see the Appendix for the derivation). Substituting (2.11) into the expression for $\mathscr{L}$ gives

$$\mathscr{L} = \frac{\lambda^2}{4(\lambda-1)}\langle (\phi' + Re)^2 \rangle + Re^2 - \frac{1}{\lambda - 1}\mathscr{H}_{\phi,\lambda}(\widehat{\boldsymbol{v}}), \tag{2.14}$$

where $\mathscr{H}_{\phi,\lambda}(\widehat{\boldsymbol{v}}) := \langle |\nabla \widehat{\boldsymbol{v}}|^2 \rangle + \lambda \langle \widehat{v}_1 \widehat{v}_3 \phi' \rangle$. A stationary value of $\mathscr{L}$ is an upper bound on ε if the minimum of the quadratic form $[1/(\lambda-1)]\mathscr{H}_{\phi,\lambda}(\widehat{\boldsymbol{v}}) = (a-1)\langle |\nabla \widehat{\boldsymbol{v}}|^2 \rangle + a\langle \widehat{v}_1 \widehat{v}_3 \phi' \rangle$

exists over the set $\mathscr{V} := \{\boldsymbol{v} \mid \boldsymbol{\nabla}\cdot\boldsymbol{v} = 0,\ \overline{\boldsymbol{v}} = \boldsymbol{0},\ \boldsymbol{v}(x, y, \pm\frac{1}{2}) = \boldsymbol{0}\}$. This means that both $a > 1$ and the so-called 'spectral' constraint

$$\mathscr{H}_{\phi,a}(\widehat{\boldsymbol{v}}) \geqslant 0 \quad \forall \widehat{\boldsymbol{v}} \in \mathscr{V} \tag{2.15}$$

must be satisfied if the stationary value of $\mathscr{L}$, calculated through solving (2.13*a–d*), is to be an upper bound on ε. The Euler–Lagrange equation for $\widehat{\boldsymbol{v}}$, (2.13*c*), implies that $\mathscr{H}_{\phi,a}(\widehat{\boldsymbol{v}}) = 0$ at every stationary point of $\mathscr{L}$ but only the largest (unique) stationary value satisfies the spectral constraint (see § 2.4 of Kerswell 1998).

Hence the upper bound which emerges from the CDH problem is

$$\mathscr{E} \leqslant \mathscr{E}_{max} := \frac{\lambda^2}{4(\lambda - 1)}\langle(\phi' + Re)^2\rangle + Re^2, \tag{2.16}$$

where ϕ and λ along with an associated fluctuation field $\widehat{\boldsymbol{v}}$ satisfy (2.13*a–d*) together with the spectral constraint.

3. Solution technique

In all studies to date no solution of the full set of Euler–Lagrange equations has been attempted. Instead test functions for ϕ have been constructed and functional inequalities on $\mathscr{H}_{\phi,a}$ used to verify the spectral constraint (Doering & Constantin 1992; Gebhardt *et al.* 1995; Nicodemus *et al.* 1997*a*). One notable exception to this is the work by Nicodemus *et al.* (1998*a*) which employs a sophisticated background trial profile with several degrees of freedom and solves the spectral constraint numerically allowing fluctuation fields with up to two spanwise wavenumbers. It remains unclear how close their solution is to the full solution.

In this section we will discuss how a numerical solution to equations (2.13*a–d*) can be found using the method of pseudo-spectral collocation (see Boyd 2001) and how the all important spectral constraint is enforced. We assume as in previous studies that the optimal solution has no streamwise variation, $\partial_x = 0$ (Busse 1969*a*, 1970). The solution to the linear equations (2.13*c*, *d*) takes the form

$$\widehat{\boldsymbol{v}} = \sum_{m=1}^{M} \begin{bmatrix} \widehat{v}_1^{(m)} \cos(k_m y) \\ \widehat{v}_2^{(m)} \sin(k_m y) \\ \widehat{v}_3^{(m)} \cos(k_m y) \end{bmatrix}, \quad \widehat{p} = \sum_{m=1}^{M} \widehat{p}^{(m)} \cos(k_m y),$$

where the hatted variables are z-dependent functions. We expand each of these functions together with the background field in Chebyshev polynomials as follows:

$$\phi(z) = -Re\, z + \sum_{n=1}^{N} \widehat{\phi}_n U_{2n}(2z) \tag{3.1a}$$

and

$$\widehat{v}_i^{(m)} = \sum_{n=1}^{N} \widehat{v}_{i,n}^{(m)} U_n(2z) \quad \text{for } i \text{ from 1 to 3}, \tag{3.1b}$$

$$\widehat{p}^{(m)} = \sum_{n=1}^{N} \widehat{p}_n^{(m)} T_{n-1}(2z), \tag{3.1c}$$

where $T_n(z)$ is the Chebyshev polynomial, $T_n(z) = \cos(n\cos^{-1}z)$, and $U_n(z)$ is the modified Chebyshev polynomial defined by $U_n(z) = T_{n+1}(z) - T_{n-1}(z)$. Every U_n

satisfies homogeneous boundary conditions by construction,

$$U_n(\pm 1) = 0 \qquad \forall n \in \mathbb{N}, \tag{3.2}$$

so this basis is a natural choice for both ϕ and $\widehat{\boldsymbol{v}}$. Under the assumption that the background field is odd in z, ϕ is expanded in the odd basis $\{U_{2n}\}$. Also, twice as much resolution is put in ϕ than $\widehat{\boldsymbol{v}}$ because ϕ' is forced by a quadratic in $\widehat{\boldsymbol{v}}$ (see equation (2.13*b*)). The equations are collocated over the interior Chebyshev grid $\{z_i = \frac{1}{2}\cos(\pi(2i-1)/(2N)), i = 1, \ldots, N\}$.

Horizontal modes do not mix because of the linearity of the optimal equation for $\widehat{\boldsymbol{v}}$ (2.13*c*) and the incompressibility constraint. Therefore these constraints separate into constraints on each subfield $[\widehat{\boldsymbol{v}}^{(m)}, \widehat{p}^{(m)}]$ as follows:

$$\frac{\delta \mathscr{L}}{\delta \widehat{\boldsymbol{v}}^{(m)}} := 2\big(\widehat{\boldsymbol{v}}^{(m)''} - k_m^2 \widehat{\boldsymbol{v}}^{(m)}\big) - \lambda\phi' \begin{bmatrix} \widehat{v}_3^{(m)} \\ 0 \\ \widehat{v}_1^{(m)} \end{bmatrix} + \begin{bmatrix} 0 \\ -k_m \widehat{p}^{(m)} \\ \widehat{p}^{(m)'} \end{bmatrix} = \mathbf{0}, \tag{3.3a}$$

and

$$k_m \widehat{v}_2^{(m)} + \widehat{v}_3^{(m)'} = 0. \tag{3.3b}$$

where $(\,)' \equiv \mathrm{d}/\mathrm{d}z$. An extra equation describing the variation of $\mathscr{L}$ with horizontal wavenumber k_m is now required to close the system of optimal equations. Expression (2.14) with the incompressibility constraint explicitly included is

$$\mathscr{L} = \frac{\lambda^2}{4(\lambda-1)}\langle(\phi' + Re)^2\rangle + Re^2 - \frac{1}{\lambda-1}[\mathscr{H}_{\phi,\lambda}(\widehat{\boldsymbol{v}}) + \langle \widehat{p}\nabla\cdot\widehat{\boldsymbol{v}}\rangle].$$

Written in terms of $\widehat{\boldsymbol{v}}^{(m)}$ and k_m we have

$$\mathscr{L} = \frac{\lambda^2}{4(\lambda-1)}\langle(\phi' + Re)^2\rangle + Re^2 - \frac{1}{\lambda-1}\sum_{m=1}^{M}\big[\big\langle \big|\widehat{\boldsymbol{v}}^{(m)'}\big|^2 + k_m^2\big|\widehat{\boldsymbol{v}}^{(m)}\big|^2 + \lambda\widehat{v}_1^{(m)}\widehat{v}_3^{(m)}\phi' + \widehat{p}^{(m)}\big(k_m\widehat{v}_2^{(m)} + \widehat{v}_3^{(m)'}\big)\big\rangle\big],$$

where $\widehat{\boldsymbol{v}}^{(m)} = [\widehat{v}_1^{(m)}, \widehat{v}_2^{(m)}, \widehat{v}_3^{(m)}]$, from which we can readily derive the k_m variation

$$\frac{\delta \mathscr{L}}{\delta k_m} := k_m\big\langle\big|\widehat{\boldsymbol{v}}^{(m)}\big|^2\big\rangle + \tfrac{1}{2}\big\langle\widehat{p}^{(m)}\widehat{v}_2^{(m)}\big\rangle = 0. \tag{3.4}$$

The only mixed mode terms in the solution of the optimal equations occur on the right-hand sides of equations (2.13*a*, *b*). These equations are now

$$\lambda = 2 - \frac{\displaystyle\sum_{m=1}^{M}\big\langle\big|\widehat{\boldsymbol{v}}^{(m)'}\big|^2 + k_m^2\big|\widehat{\boldsymbol{v}}^{(m)}\big|^2\big\rangle}{\displaystyle Re\sum_{m=1}^{M}\big\langle\widehat{v}_1^{(m)}\widehat{v}_3^{(m)}\big\rangle}, \tag{3.5a}$$

$$\lambda(\phi' + Re) = \sum_{m=1}^{M}\big[\widehat{v}_1^{(m)}\widehat{v}_3^{(m)} - \big\langle\widehat{v}_1^{(m)}\widehat{v}_3^{(m)}\big\rangle\big]. \tag{3.5b}$$

(The $\frac{1}{2}$ multiplying the left-hand side of equation (2.13a) has cancelled with one coming from integrating $\cos^2(k_m y)$.) The fact that ϕ' is even in z means that solutions to (3.3a) and (3.3b) can be sought with the pair $(\widehat{v}_1^{(m)}, \widehat{v}_3^{(m)})$ even in z and $(\widehat{v}_2^{(m)}, \widehat{p}^{(m)})$ odd in z, and vice versa. Our numerical solution of the CDH problem proceeds in two parts.

(i) *Continuation calculation from the energy stability point*

We employ a numerical continuation program called PITCON (Rheinboldt & Burkardt 1983a, b) to continue the solution of the Euler–Lagrange equations in Re from the energy stability point $Re = Re_{ES}$, when the laminar flow state ceases to be the global attractor for the Navier–Stokes equation (see Joseph 1976), through successive spanwise wavenumber bifurcations, up to asymptotically high Reynolds number. One can show that up to Re_{ES} the optimal solution of the CDH problem is the laminar solution $\phi(z) = -Re\, z$. First this ϕ, arbitrary a and $\widehat{\boldsymbol{v}} = \boldsymbol{0}$ trivially solve the Euler–Lagrange equations. Second the spectral constraint for laminar ϕ and $a = \infty$ (or equivalently $\lambda = 1$) is

$$\mathscr{H}_{\{-Re\, z, \lambda=1\}}(\widehat{\boldsymbol{v}}) = \langle |\nabla \widehat{\boldsymbol{v}}|^2 \rangle - Re \langle \widehat{v}_1 \widehat{v}_3 \rangle \geqslant 0 \qquad \forall \widehat{\boldsymbol{v}} \in V, \tag{3.6}$$

which is the condition that the laminar flow is globally asymptotically stable and holds for $Re \leqslant Re_{ES}$. At $Re_{ES} = 82.65$, the inequality in (3.6) is made marginal by an eigenfunction $\widehat{\boldsymbol{v}} = \widehat{\boldsymbol{v}}_{ES}(z)$ with the critical horizontal wavenumber $k_{ES} = 3.117$. The continuation procedure starts by setting $k_1 = k_{ES}$ and $\widehat{\boldsymbol{v}}^{(1)} = A\widehat{\boldsymbol{v}}_{ES}$, and adjusting either the amplitude A or the step size in Re until convergence occurs to a non-trivial solution.

(ii) *The spectral constraint and incoming wavenumbers*

The second part of the calculation consists of enforcing $\mathscr{H}$ to be positive-semidefinite. This so-called spectral constraint can be shown to be equivalent to solving the linear eigenvalue problem

$$2(\boldsymbol{v}'' - k^2 \boldsymbol{v}) - \lambda \phi' \begin{bmatrix} v_3 \\ 0 \\ v_1 \end{bmatrix} + \begin{bmatrix} 0 \\ -kp \\ p' \end{bmatrix} = \mu \boldsymbol{v} \tag{3.7}$$

over the space of functions $\mathscr{V}$

$$\mathscr{V} = \{\boldsymbol{v} \,|\, k v_2 + v_3' = 0, \quad \overline{\boldsymbol{v}} = \boldsymbol{0}, \quad \boldsymbol{v}\left(z = \pm\tfrac{1}{2}\right) = \boldsymbol{0}\}, \tag{3.8}$$

and verifying that $\mu \leqslant 0$ for real values of k. Here the implicit assumption is made that only streamwise-independent velocity fields are important, which is unproven but appears true (Busse 1969a, 1970; Nicodemus *et al.* 1998a). Letting $\overline{\mu}(k)$ be the maximum eigenvalue of this linear eigenvalue system at a given k, it is important to realize that the zeros of $\overline{\mu}$ correspond to fields which satisfy (3.3a, b). At $Re = Re_{ES}$, $\overline{\mu}$ has a unique maximum at $k = k_{ES}$ (i.e. $\overline{\mu}(k_{ES}) = 0$). However, as the continuation calculation proceeds by increasing Re, $\overline{\mu}(k)$ develops another maximum which if unchecked bursts through the $\mu = 0$ axis (see figure 1). Just before this occurs, that is when $\overline{\mu} \leqslant 0$ over k and $\overline{\mu}(k_1) = \overline{\mu}(k_2) = 0$ for $k_1 \neq k_2$, the continuation procedure must be stopped and the solution extended to include an extra fluctuation field $\widehat{\boldsymbol{v}}^{(2)}$ to take account of this new marginal wavenumber. The calculation is restarted by

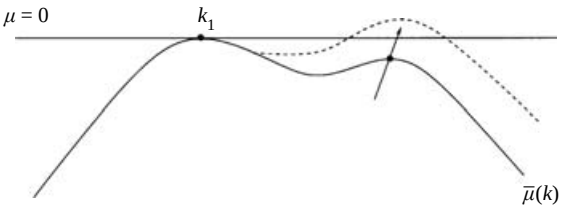

FIGURE 1. Diagram showing a new wavenumber maximum passing through the $\mu = 0$ axis.

shooting the solution into the new fluctuation field 'direction', i.e.

$$\widehat{\boldsymbol{v}}_{new} = \widehat{\boldsymbol{v}}_{old} + A \begin{bmatrix} \widehat{v}_1^{(2)} \cos(k_2 y) \\ \widehat{v}_2^{(2)} \sin(k_2 y) \\ \widehat{v}_3^{(2)} \cos(k_2 y) \end{bmatrix}. \tag{3.9}$$

The two points $\overline{\mu}(k_1)$ and $\overline{\mu}(k_2)$ are now pinned to zero through equation (3.3*a*) although the wavenumbers k_1 and k_2 change with Re. The graph of $\overline{\mu}(k)$ is again monitored to check if a third new maximum has emerged. In this way successive bifurcations are found and the number of fluctuation fields in the optimal solution gradually increases. See Doering & Hyman (1997) for an earlier numerical study in which they see evidence of the first wavenumber bifurcation in the spectral constraint.

Supplementary to finding and incorporating incoming modes, the spectral constraint eigenvalue calculation was also used as an additional test that N, the z-direction truncation, was sufficient, by checking that the M modes in the fluctuation field decomposition correspond to accurate zeros and maxima of the $\overline{\mu}(k)$ graph. The spectral calculation is independent of the optimal fluctuation field depending only on ϕ and a. So this subsidiary check of resolution is as important as checking that a higher resolution in z produces the same global properties of the optimal solution such as the dissipation rate. The background field develops a boundary layer structure near the wall which is $O(1/Re)$. As a result the truncation N required scales like $Re^{1/2}$ since the Chebyshev collocation points have an $O(1/N^2)$ spacing at the walls.

4. Results and comparison with asymptotic expressions

The main result of this work is presented in figure 2 which shows how the full-solution upper bound behaves as a function of Re. Also included for comparison are the results from the trail-function approach of Nicodemus *et al.* (1998*a*) and Busse's (1970) original asymptotics. The first observation is that the exact upper bound is indeed lower than Busse's asymptotic estimate. Furthermore, the full solution clearly does not possess the local minimum found by Nicodemus *et al.* but, rather, monotonically decreases to an asymptotic value of $\varepsilon_{bound} = 0.008553$. This plot also shows that the wavenumber bifurcation points are close to being evenly spaced in $\log(Re)$. This is a first indication that there is a self-similar structure to the spanwise wavenumbers which emerge as part of the solution. This is also clearly seen in figure 3. Incoming wavenumbers always emerge low down in the wavenumber spectrum, between k_1 and k_2 or k_2 and k_3. This property was also observed in a study by Vitanov & Busse (1997).

Unfortunately, it was only possible to find the solution up until the seventh wavenumber bifurcation ($Re = 7.33 \times 10^4$) in double precision arithmetic due to

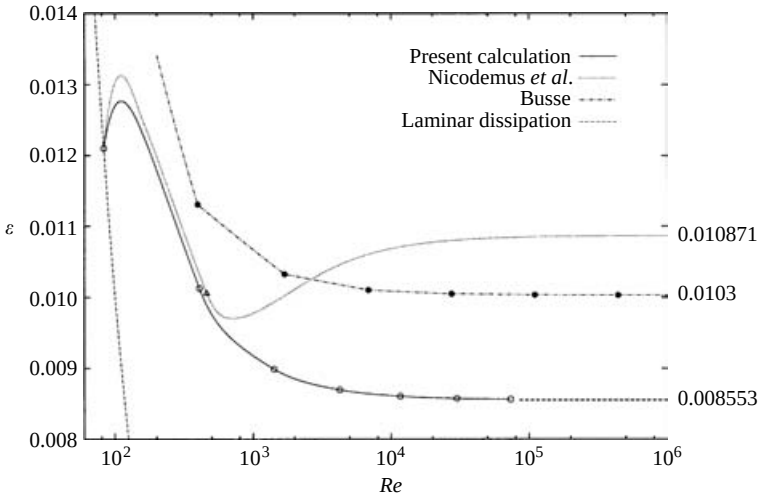

FIGURE 2. Comparison of bounds on the long-time dissipation rate ε. The dashed line shows the dissipation rate for the laminar flow state which is a theoretical minimum for ε. The dotted line is the previous best bound calculated by Nicodemus *et al.* (1998*a*). The dash-dotted line is the asymptotic Re bound of Busse (1970) extrapolated to finite Reynolds number. The solid line is the improved bound calculated here, with its extension to an asymptotic limit of 0.008553 depicted by the thick dashed line. Points represent the position of incoming modes. The open circles correspond to the wavenumber bifurcation points Re_m from this calculation, as recorded in table 1. The open triangle is the point at which Nicodemus *et al.* find a wavenumber degeneracy in their spectral constraint calculation, and the solid circles are the points of incoming wavenumbers in the multi-α solutions.

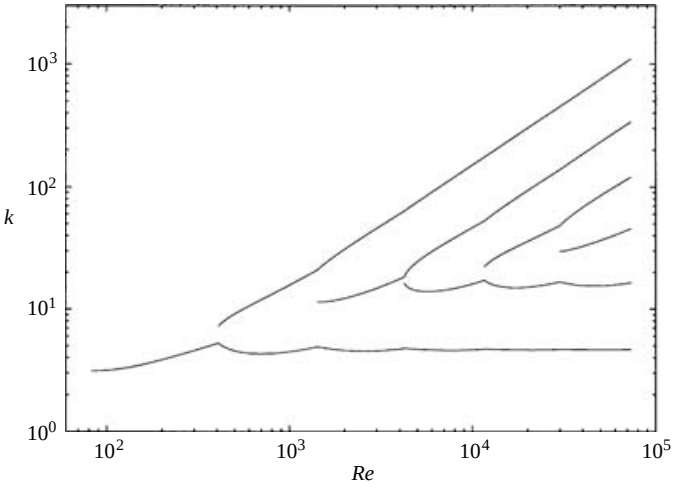

FIGURE 3. Bifurcation diagram for the spanwise wavenumber of the fluctuation field.

the sensitivity of the spectral constraint. The graph of $\overline{\mu}(k)$ at $Re = 7.33 \times 10^4$ (figure 4) shows a plateauing close to the third lowest wavenumber in $\widehat{\boldsymbol{v}}$ which is where the seventh wavenumber is emerging. In this region, $\overline{\mu} = O(10^{-5})$ and $\widehat{\nu}_i = O(10)$ so that the right-hand side of (3.7) is $O(10^{-4})$ whereas terms on the left-hand side of (3.7) are typically $O(Re^2 \sim 10^9)$ near the walls. This wide disparity

M	Re_m	N
1	82.7	8
2	407.9	12
3	1418.4	25
4	4247.5	50
5	11660.1	100
6	30004.0	200
7	73300.1	250

TABLE 1. The Reynolds numbers, Re_m, at which new wavenumbers emerge and are built into the fluctuation field, versus the total number of modes, M, and the truncation number in the z-direction, N, required to calculate the optimal solution.

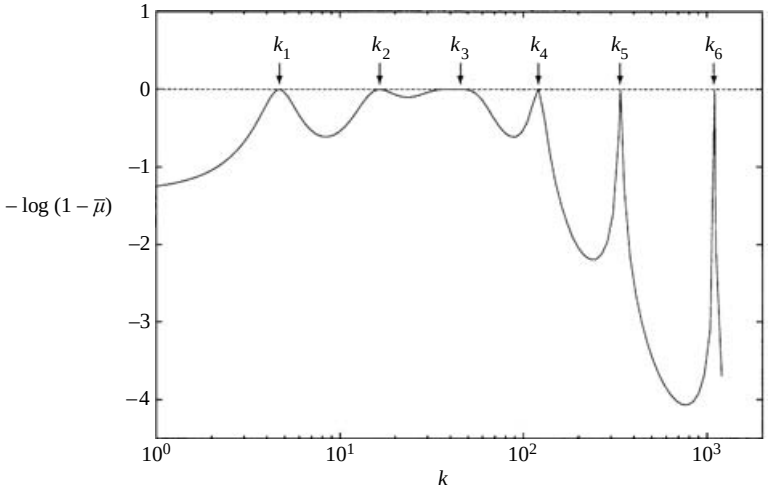

FIGURE 4. A plot of $\overline{\mu}(k)$ at $Re = 7.33 \times 10^4$ on a shifted logarithmic scale.

in scales means that the emerging zero of the spectral eigenvalue problem becomes swamped and so the narrow region of convergence for a seventh wavenumber solution is unattainable. Also at this stage the numerical effort is beginning to become an issue. At $Re = 7.32 \times 10^4$ with $N = 230$ and six wavenumbers, there were 5758 equations to be solved and every Newton–Raphson convergence took an hour on a 667MHz EV6 processor requiring 300MB of storage. An interesting feature of the continuation procedure was that PITCON automatically took smaller and smaller steps near a wavenumber bifurcation, that is, the code could sense the presence of an emerging wavenumber. Fortunately, the asymptotic behaviour of the upper bound is already clear by the seventh wavenumber bifurcation.

Further aspects of the optimizing solution are shown in figures 5 to 8. Figure 5 shows how the parameter λ starts with the value 1 when $Re = Re_{ES}$ and then converges exponentially to $\frac{3}{2}$ as $Re \to \infty$. The curve $\lambda(Re)$ is C^0 which is punctuated by discontinuities in the gradient as successive wavenumbers enter the optimal solution (see table 1). The asymptotic limit $\lambda(\infty) = \frac{3}{2}$, or equivalently $a = 3$, is predicted by Busse's (1970) asymptotics and also emerges from the numerics of Nicodemus *et al.* (1998*a*). Figures 6 and 7 show the structure of the optimal mean profile (equation (2.12)). The near-wall behaviour is emphasized in figure 6 by using traditional

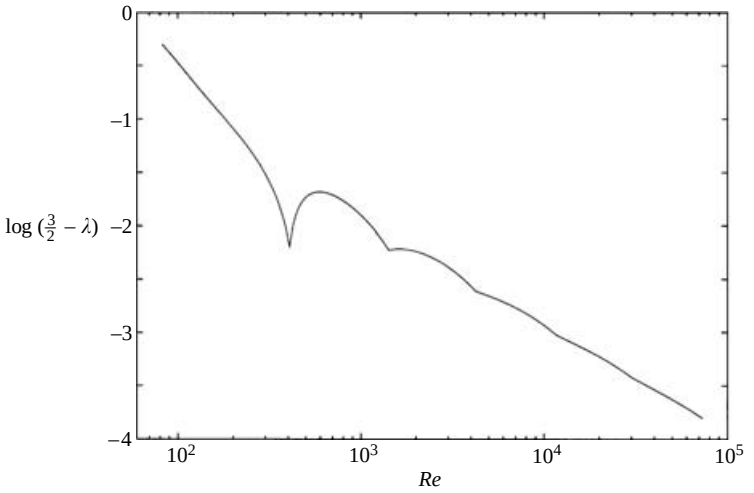

FIGURE 5. Logarithmic plot of the difference between the optimization parameter λ and its asymptotic limit $\frac{3}{2}$.

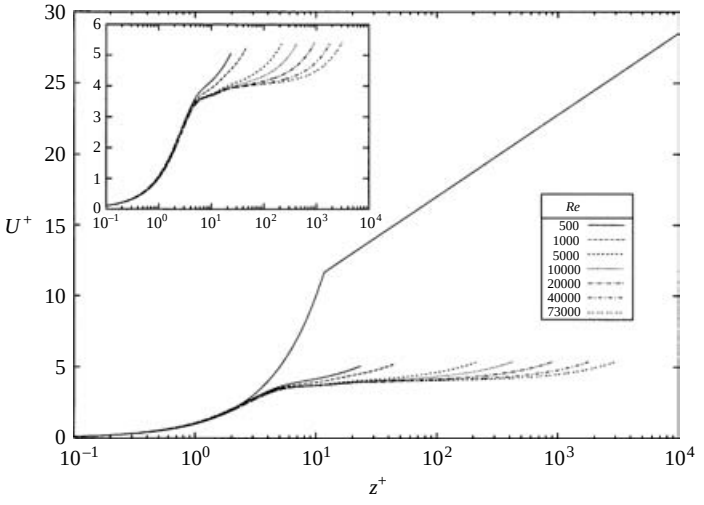

FIGURE 6. Plots of the optimal solution mean velocity in friction units for various values of *Re*. The inset shows a comparison of the mean velocity graphs only. On the main axes we plot the same optimal velocity graphs against the empirically observed mean velocity for turbulent plane Couette flow. This is defined by a viscous sublayer $U^+ = z^+$ and a logarithmic region $U^+ = 2.5 \ln z^+ + 5.5$. Our variables are $z^+ = Re_\tau(z + \frac{1}{2})$ where the friction Reynolds number $Re_\tau = \sqrt{\mathscr{E}/Re}$, and $U^+ = U/U_\tau$ where U is the change in mean velocity away from the wall $U = \frac{1}{2}Re - \overline{\boldsymbol{u}} \cdot \hat{\boldsymbol{x}}$, and $U_\tau = \sqrt{\mathscr{E}/Re}$ is the friction velocity length scale.

friction units. This clearly shows that the optimal mean profile does not have any logarithmic region outside the viscous sublayer, as observed experimentally. The boundary layer is tighter than for real flows and the region outside this is flat rather than following a logarithmic increase. Figure 7 shows the characteristic $\frac{1}{4}$-shear through the interior (i.e. the shear is a $\frac{1}{4}$ of the laminar value) which is predicted by Busse's asymptotics and found also by Nicodemus *et al.* (1998*a*). Figure 8 illustrates

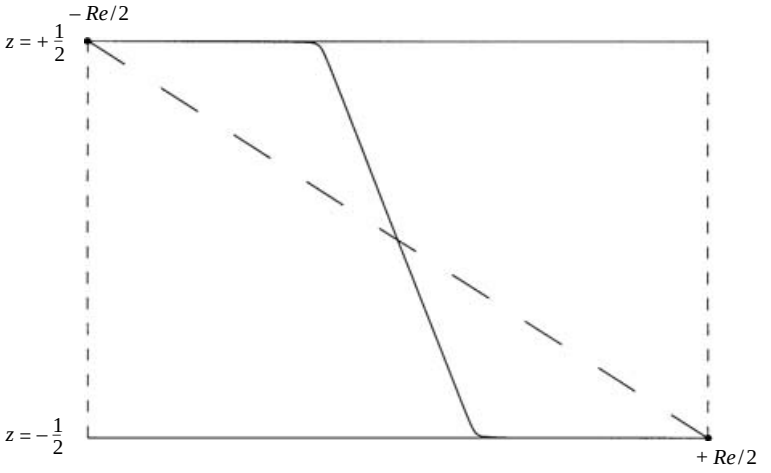

FIGURE 7. A plot of the mean velocity profile at $Re = 7.33 \times 10^4$ which clearly shows a channel interior gradient of $\frac{1}{4}Re$, which in inviscid units is $\frac{1}{4}$. The long-dashed line is the laminar flow profile. This means that the mean velocity profile has an unphysical $\frac{1}{4}$-shear in common with Busse's multi-α solutions.

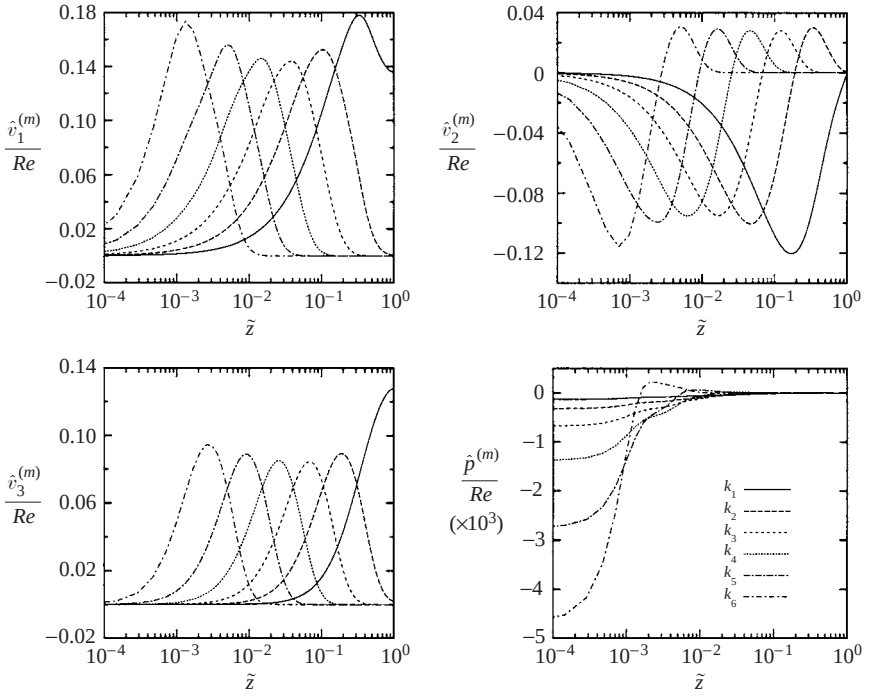

FIGURE 8. Plots of the z-dependent subfields of the fluctuation field at $Re = 7.33 \times 10^4$ where $\tilde{z} = 2z + 1$. The key for all of the plots is given in the pressure plot.

the self-similarity of the various velocity fields associated with the wavenumbers, which is consistent with Busse's asymptotics. These fields all have the parity of $(\widehat{v}_1^{(m)}, \widehat{v}_3^{(m)})$ both even and $(\widehat{v}_2^{(m)}, \widehat{p}^{(m)})$ both odd because this parity of solution turned out to be the most critical in the spectral constraint.

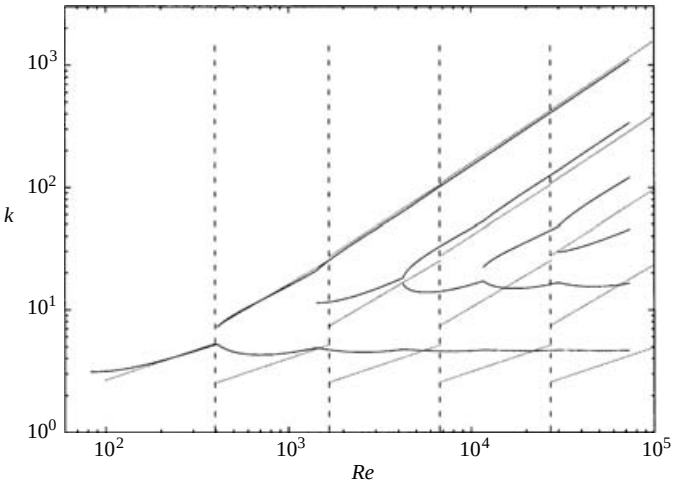

FIGURE 9. A comparison between the wavenumbers of the optimal solution and those in Busse's multi-α solutions. The dashed vertical lines indicate the points of incoming modes in the multi-α solution, which are seen to occur later than the corresponding points for the optimal solution.

Further comparisons can be made with Busse's multiple-boundary-layer analysis which identifies the asymptotic behaviour of N boundary layer trial-function solutions and their corresponding upper bounds $\varepsilon_N(Re)$ for $N \in \mathbb{N}$. Theoretically, each provides a lower estimate of the correct upper bound so that the highest such (as a function of Re) is of most interest. Figure 2 shows the bound corresponding to this estimate as Re varies and, since ε_N scales as $Re^{-4^{-N}}$, the curve is piecewise linear. (Technically, of course, Busse's results are only asymptotic but it is difficult to resist plotting their predictions down to finite Re nevertheless.) Figure 9 presents a comparison of the wavenumber bifurcation structure revealed here with that predicted by Busse. There is generally good agreement, with the asymptotics capturing the largest wavenumber (corresponding to the innermost boundary layer structure) well. On the other hand, the asymptotics fails to reproduce the lowest wavenumber, which is almost constant and $O(1)$. Also, by the largest Re reached here, the asymptotics only predict five wavenumbers in the solution whereas, in fact, in the true solution the seventh is just about to appear.

5. Discussion

This paper presents a complete solution to the CDH problem to when the seventh wavenumber bifurcation occurs at $Re = 73\,300$. By this point, the asymptotic value of the upper bound can be predicted to be $\varepsilon_{bound} = 0.008553$, thereby improving the previous best bound found by Nicodemus *et al.* (1998*a*) by 21%. It is also clear that their use of a restricted form for the background field gives rise to anomalous behaviour in their results. Specifically, the global minimum that they find at $Re \approx 740$ is not a true feature of the exact bound. We also confirm that Busse's multiple-boundary-layer estimate is 17% too high. This discrepancy can be attributed to the neglect of supposedly 'higher order' terms in the derivation of the multiple-boundary-layer solutions. In a little known technical report Busse (1968*b*) estimated that there was

a possible 20% margin of error in his upper bound result published in 1970, that is

$$0.8\,\varepsilon_{Busse} \approx \frac{1}{124.6} \leqslant \varepsilon_{bound} \leqslant \varepsilon_{Busse} \approx \frac{1}{99.7} \quad \text{as } Re \to \infty. \tag{5.1}$$

Since we have found $\varepsilon_{bound} = 0.008553 \approx 1/116.9$, this estimate now looks spot on.

More generally, we have confirmed that Busse's multiple-boundary technique for attacking the CDH variational problem does appear to capture the main features of the exact solution. These features include the fact that the solution develops an increasing number of nestled boundary layers corresponding to successive wavenumber bifurcations, that the velocity structures associated with each is self-similar and that the optimal mean flow assumes a $\frac{1}{4}$-shear profile. This success bodes well for other applications of this technique in different variational problems (Kerswell 2002). We have also confirmed that the optimal mean profile does not exhibit a logarithmic layer beyond the viscous sublayer. Given the consensus view that there is vanishing interior shear at asymptotically large Re (although see Busse 1996 for a counter view), this means that the CDH variational problem only manages to capture the first (fairly trivial) essence of experimentally observed turbulent mean profiles – a viscous sublayer – albeit perhaps a factor of 3 thinner than it should be. The conclusion, if any has to be drawn, is that there is no evidence to support the hypothesis that a real turbulent flow tries to optimize the momentum transport (or equivalently the energy dissipation rate) between the plates.

We make the remark that the CDH variational problem is now exhausted. The best asymptotic bound calculated here ($\varepsilon < 0.008553$) represents just over a factor of 10 improvement on the original estimate by Doering & Constantin (1992) ($\varepsilon < 1/8\sqrt{2} \approx 0.08839$) found 10 years ago. New constraints will have to be added if this result is to be improved further.

Finally, it is worth remarking that the new upper bound derived in this paper can be converted in to an upper bound for arbitrary-Prandtl-number Boussinesq convection in the same geometry using techniques described in Section IV of Kerswell (2001). The upper bound result reported here, $\varepsilon \leqslant 0.008553$ as $Re \to \infty$, is formally equivalent to the upper bound on the Nusselt number $Nu - 1 \leqslant 0.02634 Ra^{1/2}$ as $Ra \to \infty$.

We are grateful to F. H. Busse for bringing his 1968*b* report to our attention and along with C. Caulfield and C. Doering for many helpful comments on this manuscript. Thanks also to M. Holthaus for providing the numerical data from figure 8 of Nicodemus *et al.* (1998*a*) which is presented in our figure 2 for comparison purposes. We both gratefully acknowledge the support of the EPSRC.

Appendix

We show here how to deduce expression (2.13*a*) starting from the variational derivative for a (equation 2.9*a*). In what follows, we will use the formula for the mean of $\boldsymbol{v}$ (equation (2.11)), the product $\langle \widehat{\boldsymbol{v}} \cdot \delta\mathscr{L}/\delta\widehat{\boldsymbol{v}} \rangle = 0$,

$$\langle |\nabla\widehat{\boldsymbol{v}}|^2 \rangle = -\lambda \langle \phi' \widehat{v}_1 \widehat{v}_3 \rangle, \tag{A 1}$$

and the equation for the background field (equation (2.13*b*)). Substituting $\boldsymbol{v} = \widehat{\boldsymbol{v}} + \overline{v_1}\widehat{\boldsymbol{x}}$ into equation (2.9*a*) and using equation (2.11) we find that

$$\langle |\nabla\widehat{\boldsymbol{v}}|^2 + \frac{(\lambda-2)^2}{4}(\phi' + Re)^2 + \phi'\widehat{v}_1\widehat{v}_3 + \frac{\lambda-2}{2}\phi'(\phi' + Re) \rangle = 0.$$

Now by separating the product $(\phi' + Re)^2$ by using equation (2.13*b*) once only,

$$(\phi' + Re)^2 = \frac{2}{\lambda}(\phi' + Re)(\overline{\widehat{\nu}_1\widehat{\nu}_3} - \langle\widehat{\nu}_1\widehat{\nu}_3\rangle),$$

we are lead to the following:

$$\left\langle |\nabla\widehat{\boldsymbol{v}}|^2 + \frac{1}{2\lambda}[(\lambda-2)^2\phi'(\overline{\widehat{\nu}_1\widehat{\nu}_3} - \langle\widehat{\nu}_1\widehat{\nu}_3\rangle) + 2\lambda\phi'\overline{\widehat{\nu}_1\widehat{\nu}_3} + 2(\lambda-2)\phi'(\overline{\widehat{\nu}_1\widehat{\nu}_3} - \langle\widehat{\nu}_1\widehat{\nu}_3\rangle)] \right\rangle = 0,$$

which simplifies to

$$\langle |\nabla\widehat{\boldsymbol{v}}|^2 + \tfrac{1}{2}[(\lambda-2)\phi'(\overline{\widehat{\nu}_1\widehat{\nu}_3} - \langle\widehat{\nu}_1\widehat{\nu}_3\rangle) + 2\phi'\overline{\widehat{\nu}_1\widehat{\nu}_3}] \rangle = 0.$$

Now exploiting $\langle\phi'\rangle = -Re$, which is a direct consequence of the boundary conditions on ϕ, we may rewrite this as

$$\langle |\nabla\widehat{\boldsymbol{v}}|^2\rangle + \tfrac{1}{2}[\lambda\langle\phi'\overline{\widehat{\nu}_1\widehat{\nu}_3}\rangle - (2-\lambda)Re\langle\widehat{\nu}_1\widehat{\nu}_3\rangle] = 0$$

and then use equation (A 1) to recover the result

$$\lambda = 2 - \frac{\langle |\nabla\widehat{\boldsymbol{v}}|^2\rangle}{Re\langle\widehat{\nu}_1\widehat{\nu}_3\rangle}.$$

REFERENCES

Boyd, J. P. 2001 *Chebyshev and Fourier Spectral Methods*, 2nd edn. Dover.

Busse, F. H. 1968*a* Eine neuartige Methode zur theoretischen Behandlung turbulenter Transportvorgänge. *Z. Angew. Math. Mech.* **48**, T187–T190.

Busse, F. H. 1968*b* On the mean field problem of thermal convection. *Tech. Rep.* 8. Max-Planck-Institut für Physik und Astrophysik.

Busse, F. H. 1969*a* Bounds on the transport of mass and momentum by turbulent flow. *Z. Angew. Math. Phys.* **20**, 1–14.

Busse, F. H. 1969*b* On Howard's upper bound for heat transport by turbulent convection. *J. Fluid Mech.* **37**, 457–477.

Busse, F. H. 1970 Bounds for turbulent shear flow. *J. Fluid Mech.* **41**, 219–240.

Busse, F. H. 1978 The optimum theory of turbulence. *Adv. Appl. Mech.* **18**, 77–121.

Busse, F. H. 1996 Bounds for properties of complex systems. In *Nonlinear Physics of Complex Systems – Current Status and Future Trends* (ed. J. Parisi, S. Müller & W. Zimmermann). Springer.

Constantin, P. & Doering, C. R. 1995 Variational bounds on energy-dissipation in incompressible flows: II. Channel flow. *Phys. Rev.* E **51**, 3192–3198.

Doering, C. R. & Constantin, P. 1992 Energy dissipation in shear driven turbulence. *Phys. Rev. Lett.* **69**, 1648–1651.

Doering, C. R. & Constantin, P. 1994 Variational bounds on energy dissipation in incompressible flows: Shear flow. *Phys. Rev.* E **49**, 4087–4099.

Doering, C. R. & Constantin, P. 1996 Variational bounds on energy dissipation in incompressible flows: III. Convection. *Phys. Rev.* E **53**, 5957–5981.

Doering, C. R. & Hyman, J. M. 1997 Energy stability bounds on convective heat transport: numerical study. *Phys. Rev.* E **55**, 7775–7778.

Gebhardt, T., Grossmann, S., Holthaus, M. & Löhden, M. 1995 Rigorous bound on the plane-shear-flow dissipation rate. *Phys. Rev.* E **51**, 360–365.

Hopf, E. 1941 Ein allgemeiner endlichkeitssatz der hydrodynamik. *Mathematische Annalen* **117**, 764–775.

Howard, L. N. 1963 Heat transport by turbulent convection. *J. Fluid Mech.* **17**, 405–432.

Howard, L. N. 1972 Bounds on flow quantities. *Annu. Rev. Fluid Mech.* **4**, 473–494.

Howard, L. N. 1990 Limits on the transport of heat and momentum by turbulent convection with large scale flow. *Stud. Appl. Maths* **83**, 273–285.

Joseph, D. D. 1976 *Stability of Fluid Motions I*. Springer.

Kerswell, R. R. 1997 Variational bounds on shear-driven turbulence and turbulent Boussinesq convection. *Physica* D **100**, 355–376.

Kerswell, R. R. 1998 Unification of variational principles for turbulent shear flows: the background method of Doering–Constantin and Howard–Busse's mean-fluctuation formulation. *Physica* D **121**, 175–192.

Kerswell, R. R. 2001 New results in the variational approach to turbulent Boussinesq convection. *Phys. Fluids* **13**, 192–209.

Kerswell, R. R. 2002 Upper bounds on general dissipation functionals in turbulent shear flows: revisiting the 'Efficiency' functional. *J. Fluid Mech.* **461**, 239–275.

Malkus, W. V. R. 1954 The heat transport and spectrum of thermal turbulence. *Proc. R. Soc. Lond.* A **225**, 196–212.

Malkus, W. V. R. 1956 Outline of a theory for turbulent shear flow. *J. Fluid Mech.* **1**, 521–539.

Nicodemus, R., Grossmann, S. & Holthaus, M. 1997*a* Improved variational principle for bounds on energy dissipation in turbulent shear flow. *Physica* D **101**, 178–190.

Nicodemus, R., Grossmann, S. & Holthaus, M. 1997*b* Variational bound on energy dissipation in plane Couette flow. *Phys. Rev.* E **56**, 6774–6786.

Nicodemus, R., Grossmann, S. & Holthaus, M. 1998*a* The background flow method. Part 1. Constructive approach to bounds on energy dissipation. *J. Fluid Mech.* **363**, 281–300.

Nicodemus, R., Grossmann, S. & Holthaus, M. 1998*b* The background flow method. Part 2. Asymptotic theory of dissipation bounds. *J. Fluid Mech.* **363**, 301–323.

Rheinboldt, W. C. & Burkardt, J. V. 1983*a* ALGORITHM 596, a program for a locally parameterized continuation process. *ACM Trans. Math. Software* **9**, 236–241.

Rheinboldt, W. C. & Burkardt, J. V. 1983*b* A locally parametrized continuation process. *ACM Trans. Math. Software* **9**, 215–235.

Vitanov, N. K. & Busse, F. H. 1997 Bounds on the heat transport in a horizontal layer with stress-free boundaries. *Z. Angew. Math. Phys.* **48**, 310–324.